Lawrence Berkeley Laboratory
UNIVERSITY OF CALIFORNIA

Materials & Molecular Research Division

Submitted to the Journal of Materials Science

INITIATION OF MODE I DEGRADATION IN SODIUM-BETA ALUMINA ELECTROLYTES

L.A. Feldman and Lutgard C. De Jonghe

April 1981

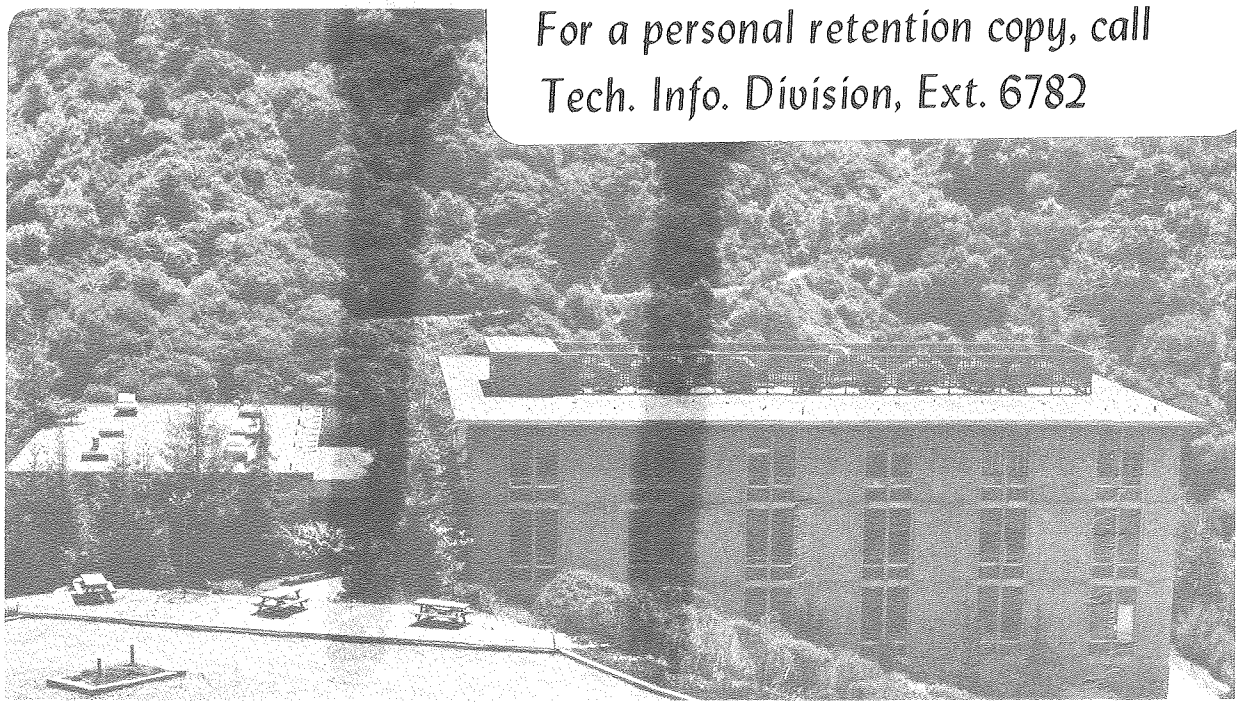

Prepared for the U.S. Department of Energy under Contract W-7405-ENG-48

DISCLAIMER

INITIATION OF MODE I DEGRADATION IN SODIUM-BETA ALUMINA ELECTROLYTES

L. A. Feldman * ‡ and Lutgard C. De Jonghe * ≠

*Materials and Molecular Research Division
Lawrence Berkeley Laboratory

and

≠ Department of Materials Science and Mineral Engineering
University of California
Berkeley, California 94720

April, 1981

This work was supported by the Electric Power Research Institute. Additional support was received from the Assistant Secretary for Conservation and Solar Energy, Office of Advanced Conservation Technology, Electrochemical Systems Research Division of the U. S. Department of Energy under Contract No. W-7405-Eng-48.

---

‡ Present address: Aerospace Corporation, P. O. Box 92957, Los Angeles, California 90009. Materials Sciences Laboratory

INITIATION OF MODE I DEGRADATION IN SODIUM-BETA ALUMINA ELECTROLYTES

L. A. Feldman*‡ and Lutgard C. De Jonghe*†

*Materials and Molecular Research Division
Lawrence Berkeley Laboratory

and

†Department of Materials Science and Mineral Engineering
University of California
Berkeley, California 94720

ABSTRACT

Current focusing resulting in extension of initial surface cracks in beta alumina electrolytes (Mode I degradation) is discussed in terms of existing models. Focusing for an ion current impinging on an elliptic-cylindrical flaw is calculated by solving for the electric potential with suitable boundary conditions. The current density distribution along the crack is used to calculate the sodium flow velocity and Poiseuille pressure inside the flaw. Calculated critical current densities using a K_{IC} criterion are several orders of magnitude higher than measured average critical current densities. This implies a lower effective K_{IC} for electrolytic degradation than for mechanical testing. Current density enhancement around insulating barriers, such as non-wetted surface areas, is also calculated using elliptic-

---

‡Present address: Aerospace Corporation, P.O. Box 92957, Los Angeles, California 90009. Material Sciences Laboratory.

cylindrical coordinates. Significant current density enhancements are found, but they are localized in very small regions. Crack growth would occur within these regions, but should be arrested once the flaw extends past the high current density zone. A plausible mechanism for decreasing K_{IC} in the electrolytic case is discussed.

1. INTRODUCTION

The degradation of sodium-beta and beta" alumina fast ion conductors during cycling in sodium/sulfur cells may occur by different mechanisms [1]. Mode I degradation is the penetration of the electrolyte by a sodium filled crack or crack network propagated through the electrolyte from the sodium/beta alumina interface, driven by cathodic plating of sodium into the crack. In contrast to Mode I, Mode II degradation results from the formation of sodium metal in the bulk of the solid electrolyte as a consequence of the development of some electronic conduction. For Mode I, the local cathodic deposition of sodium is enhanced by the crack geometry. A specific calculation requires assuming a specific crack geometry. As was indicated by De Jonghe et al. [2], this crack geometry may be complicated in the propagation phase where frequently crack branching may be observed. For the purpose of calculating current density thresholds for initiation of Mode I, the assumption that a single, small, sodium-filled surface crack is the active defect appears to be quite plausible.

In the first treatment of the Mode I breakdown problem by Armstrong et al. [3], the electrolyte was modelled as a parallel sided slab with a sodium filled flaw extending perpendicular to the sodium/electrolyte interface. The flaw was then considered to take the form of a hemispherically capped cylinder. The current flowing into the flaw was obtained by assuming the sodium metal to be at the same potential everywhere, and by calculating an effective resistance around the tip of the crack. This approximate treatment gave the qualitative result that the crack growth velocity is proportional to the crack

length and to the average current density in the slab, but it did not make use of critical fracture concept and did not yield a "threshold" current density below which degradation of this type will not occur.

A more refined treatment has been given by Shetty et al. [4], in which the crack shape was calculated using elasticity theory such that its shape was consistent with the pressure generated due to the viscous flow of the sodium within. A crack profile-pressure distribution was then determined by an iterative calculation reaching self consistent results. The finding was that the profile changed little after the first iteration, given an approximately parallel sided crack with rounded tip and a uniform pressure gradient. By incorporating the critical fracture concept together with the linear pressure profile, large current densities were calculated to be necessary for crack extension. The current densities were on the order of 1500 A/cm^2 for an initial flaw length 25 μm in beta" alumina. This is about a factor of 10^3 larger than the typical average current densities that are observed for the initiation of rapid breakdown by Mode I.

A more accurate treatment is given here for the current focusing and fracture problem, in that it calculates directly the primary current density distribution and sodium pressure along that crack. Some simplification in the analysis is achieved by using an elliptic-cylindical crack shape. This further refinement of the current focusing problem leads to a critical current density that is even higher than the ones calculated in the more approximate treatments.

2. CURRENT FOCUSING - SODIUM FLOW VELOCITY

The calculation is performed for a crack of elliptic-cylindrical shape, as shown in Figure 1. The equation $\nabla^2 \phi = 0$ is readily solved in elliptic-cylindrical coordinates in terms of elementary functions [5], and it remains only to tailor the boundary conditions fitting the present problem to determine the particular solution. The crack coordinate system and geometry are indicated in Figure 2. The elliptic-cylindrical coordinates are defined by

$$\begin{aligned} x &= a \cosh \eta \cos \psi \\ y &= a \sinh \eta \sin \psi \\ z &= z \end{aligned} \tag{1}$$

The crack parameters of length, ℓ, and one-half the crack opening displacement, r, are given by

$$\begin{aligned} \ell &= a \cosh \eta_o \\ r &= a \sinh \eta_o \end{aligned} \tag{2}$$

The potential is chosen to satisfy the uniform field condition at infinity $\phi = E_\infty x$, while at the sodium/electrolyte interface, $\phi = o$. The potential inside the electrolyte is then found to be:

$$\phi = \frac{E_\infty a \cos \psi}{\cosh \eta_o - \sinh \eta_o} (\cosh \eta_o \sinh \eta - \sinh \eta_o \cosh \eta) \tag{3}$$

The field is obtained from $\vec{E} = - \vec{\nabla} \phi$ in elliptic-cylindrical coordinates. The current density flowing through the surface of the crack ($\eta = \eta_o$) is

$$j = \frac{j_\infty \cos\eta \,(\cosh\eta_o + \sinh\eta_o)}{(\cosh^2\eta_o - \cos^2\eta)^{1/2}} \tag{4}$$

where $j_\infty = \sigma E_\infty$.

The current density at the tip ($\psi = 0$) for a narrow crack ($r/\ell << 1$) is

$$j_{max} = j_\infty (1 + \coth\eta_o) \simeq j_\infty \ell/r \tag{5}$$

This value is a factor of two smaller than the one obtained by the approximate treatments of Richman and Tennenhouse [6].

From the current density distribution, the total sodium flux versus distance along the crack can be found, yielding an average flow velocity that is independent of position along the crack. This is a consequence of the elliptic crack geometry and simplifies the calculation. The current contribution, $j(\psi)$, per unit width, w, along z for an element of arc along the crack surface is

$$\frac{di(\psi)}{w} = 2j\,(\psi)\, dS \tag{6}$$

where $dS = a\,(\cosh^2\eta_o - \cos^2\eta_o)^{1/2} d\psi$.

The factor of 2 arises since the current is fed in from both sides of the crack. Substitution for $j(\psi)$ from Eqn. (4) and integration gives:

$$i(\psi)/w = 2j_\infty\, a\,(\cosh\eta_o + \sinh\eta_o) \int_0^\psi \cos\psi\, d\psi$$

or

$$i(\psi)/w = 2j_\infty\, a\,(\cosh\eta_o + \sinh\eta_o) \sin\psi \tag{7}$$

The total current into the crack ($\psi = \pi/2$) per unit width is approximately $2j_\infty a$, which compares well with the estimate of Richman and Tennenhouse [6]. The flow velocity is related to the ratio of the flux through a cross section of the crack to the cross sectional area, $i(\psi)/2wy(\psi)$. This average flux $\bar{j}$ is given by

$$\bar{j} = \frac{j_\infty a (\cosh \eta_o + \sinh \eta_o)}{\sinh \eta_o} \tag{8}$$

The flow velocity for sodium, $\bar{v}$, is determined from the relation $\bar{j} = ne\bar{v}$ where n is the atom number density of liquid sodium and e is the sodium ionic charge. Thus

$$\bar{v} = v_\infty (1 + \coth \eta_o) \tag{9}$$

where $v_\infty = j_\infty/ne$. Thus, the velocity $\bar{v}$ is independent of position along the elliptic-cylindrical crack.

3. FLOW PRESSURE AND FRACTURE MECHANICS OF CRACK

The flow pressure is calculated, assuming Poiseuille type viscous flow along x between infinite parallel plates of spacing 2y:

$$\frac{dP}{dx} = \frac{-3 \tau \bar{v}}{y^2} \tag{10}$$

where τ is the viscosity and $\bar{v}$ is the average flow velocity. This will be in reasonable agreement with the present geometry away from the tip of a long, narrow crack with nearly parallel faces.

In the high curvature region at the tip, the flow will be more nearly perpendicular to the walls. The assumption that $\bar{v}$ is given by Eqn. (9) up to the crack tip should over-estimate the pressure gradient near the tip, thus giving an upper bound on the pressure. The gradient is:

$$\frac{dP}{dx} = \frac{-3\,\tau\,v}{a^2 \cdot \sinh^2\eta_o \cdot \sin^2\eta} \tag{11}$$

or

$$\frac{dP}{dx} = \frac{-3\,\tau\,\bar{v}}{a^2 \cdot \sinh^2\eta_o \cdot (1-x^2/\ell^2)}$$

Assuming P = 0 at x = 0, we integrate to find P(x)

$$P(x) = -P_o \tanh(x/\ell) \tag{12}$$

where $P_o = 3\,\tau\,\bar{v}\ell/r^2$, which is the pressure head developed along a parallel sided channel of spacing 2r. This is the pressure head value of Shetty et al [4]. The two pressure distributions are compared in Figure 3.

In terms of a fracture mechanics approach, K_I must be evaluated for this internally loaded crack. It is given for an internally loaded edge crack [7] by

$$K_I = \frac{2}{\pi}\int_0^{\ell} \frac{[1 + f\,(x/\ell)]\,\ell^{1/2}\,P(x)}{(\ell^2 - x^2)^{1/2}}\,dx \tag{13}$$

with $f(u) = (1 - u)\,(0.2945 - 0.3912u^2 + 0.7685u^4 - 0.9942u^6 + 0.5094u^8)$. Equation (13) is an integral form of the formula for K_I given by Sih [7] for loading by a point force. Substitution of P(x) from (12) reduces the problem to evaluating a series of convergent integrals of the form

$$\int_0^1 q^n\,(1 - q^2)^{-1/2}\,\ln\left(\frac{1 + q}{1 - q}\right) dq$$

which are transformed, by substituting $y = \ln\ (1 + q)/(1 - q)$, into integrals of the form:

$$1/2 \int_0^\infty \frac{y\,\tanh^{\,n}(y/2)}{\cosh\,(y/2)}\,dy$$

These integrals can be approximated numerically using Simpson's rule. The result (for $r/\ell \ll 1$) is:

$$K_I = \frac{3.783\ \ell^{1/2} P_o}{\pi}$$

or

$$K_1 = \frac{11.35}{\pi}\ \tau(\ell/r)^3 \ell^{\ -1/2} v_\infty \qquad (14)$$

Some results from fracture mechanics on the relation of crack displacement to length in a generalized crack geometry [8] may be used to eliminate r from Eqn. (14). This yields (see Appendix A)

$$r = (4k/3)^{1/4}\ \ell^{3/4} \qquad (15)$$

where $k = \frac{2}{E'}\,\frac{11.35\,\tau}{\pi^{3/2}}\,v_\infty$

E' is the Young's modulus. This gives

$$K_I = 1.35\ E'^{\,3/4}\ (\tau\ v_\infty\ \ell\ )^{1/4} \qquad (16)$$

or

$$K_I = 1.35\ E'^{\,3/4}\ (\tau/ne)^{1/4}\ (j_\infty\ \ell)^{1/4}$$

and

$$j_{crit} = K_{IC}^{\,4}\ E'^{-3}\ ne/(3.32\ \tau\ \ell) \qquad (17)$$

An illustration of some typical values of the crack parameters is shown in Table I. The values of the constants used are $E' = 10^5$ MPa, $\tau = 0.34$ centipoise for sodium at 300°C, and $ne = 4.2 \times 10^9$ coul/m^3. For comparison the mechanically determined K_{IC} is about 1.6×10^6 MPa $m^{1/2}$ [4]. As can be seen, the critical current densities for cracks of reasonable length are very high compared to the typical values that are observed for electrolyte failure by Mode I.

4. CURRENT ENHANCEMENT AROUND A BLOCKING REGION

The problem of current distribution around a blocking layer in a solid electrolyte has been described by Virkar et al. [9] using a mechanical analog of the current flow problem. It may also be treated directly as in the previously discussed example by choosing a suitable geometry in which Laplace's equation may be solved. In this case, an example of a blocking layer would be a portion of the electrolyte/sodium interface which is non-conducting, such as a non-wetted region or an unfavorably oriented plate-like crystallite in the surface. An elliptic-cylindrical geometry for the insulating barrier can be used again, and Laplace's equation is solved in elliptic-cylindrical coordinates. The flaw geometry and current flow orientation are shown in Figure 4. The coordinates

and crack parameters are the same as in the earlier example. The field far from the platelet is parallel to the y-axis and the condition on the potential at infinity is $\phi = E_\infty y$. The other conditions are that $\phi = 0$ in the x-z plane ($\psi = 0,\pi$) and the normal derivative of the potential vanishes at the platelet surface, $\partial\phi/\partial\eta = 0$ where $\eta=\eta_o$. The potential inside the electrolyte is given by

$$\phi= \frac{E_\infty \sin \psi \, (\cosh \eta_o \cosh \eta - \sinh \eta_o \sinh \eta)}{(\cosh \eta_o - \sinh \eta_o)} \tag{18}$$

from which the electric field and current density are determined directly. The magnitude of the current density normal to the electrolyte surface flowing in the x-z plane ($\psi = 0, \pi$) is

$$j_y = j_\infty \frac{\coth \eta \coth \eta_o - 1}{\coth \eta_o - 1} \tag{19}$$

The magnitude of the current density enhancement j_{max}, at the edge of the platelet ($\eta = \eta_o$; $\psi = 0, \pi$) is

$$\begin{aligned} j_{max} &= j_\infty (\coth \eta_o + 1) \\ &\simeq j_\infty \ell/r \end{aligned} \tag{20}$$

This current density enhancement around the edge of the platelet is a factor of two smaller than the one obtained by Virkar et al. [9] from the mechanical analog of the problem.

An illustration of the qualitative nature of the mechanical analog for the current density can be made by comparing the tangential stress around an elliptical hole in a sheet under uniaxial tension and the tangential current density around an identical hole in a conducting

sheet with a uniform current density at infinity in place of the uniaxial tension. Figure 5 shows the comparison between the calculated normalized tangential stress, as given in Jaeger [10] and the normalized tangential current density around the hole calculated as described above for $r/\ell = 1/2$. Thus we see that the mechanical analog is not exact in geometrics such as these. For example, the calculated mechanical stress enhancement at the point of highest curvature around the hole shown in Figure 5 is 5/3 times the electrical current density enhancement at the same point; the analog tends to exaggerate the current density enhancement.

It is necessary to know the spatial extent of the zone of enhanced current density around the platelet. This allows an estimate of the increased current focusing experienced by an initial flaw situated at the edge of a platelet. From the relation of current density to position along the electrolyte/metal electrode interface the maximum current density is formed to occur at the platelet edge and to decrease smoothly to the value j_∞ far from the platelet. Let us now take the current density to be uniform in the current enhanced region, instead of decreasing, with a value of $j_{max} \simeq j_\infty \ell/r$. Let us also take the current density to be uniform outside the enhanced region, with a value of j_∞. Since the boundary condition of uniform current density of magnitude j_∞at large y imposes a definite total current, the conservation of current (Kirchoff's Law) determines the width, R, of the high field or high current region. The total current in that region, $j_{max}Rw$, must be, to a first approximation, $1/2(2j_\infty \ell w)$, for $r/\ell << 1$, which would be half the current flowing through the platelet

area if the blocking platelet were removed. The current flowing around the platelet is in a sense a "displaced" current. Equating the current in the enhanced zone with the total displaced current gives a zone of width $j_\infty \ell / j_{max}$, or r. Thus, for $r/\ell << 1$ and large current density enhancement, the zone size is also very small compared to the length of the platelet. A somewhat more exact argument, which gives the same basic result can be made by finding the point of intersection of the tangents to the integrated current versus position curve. The tangents to the curve are constructed at the platelet edge and at infinity, on the interface. Figure 6 indicates schematically an initial flaw located at the edge of a blocking platelet in the enhanced current region.

Table II gives the values of j_{crit} for several assumed initial flaw lengths, L_c, and the approximate zone size, R, of the enhanced current density region near the platelet edge where the current density exceeds j_{crit}. The insulating platelet size was taken to be 1 cm, r/ℓ was 10^{-7}, and j_∞ was 1 A/cm^2. The zone dimension R was estimated from a calculation of j_y using Eqn. 19. It could also be obtained from the approximation of Eqn. 19 since $j_y/j_\infty \simeq (\ell/2R)^{1/2}$, for $r/\ell < (2R/\ell)^{1/2} << 1$.

It is seen that the current enhancement zones are many orders of magnitude too small, or that the experimentally observed critical currents of a few A/cm^2 are many orders of magnitude lower than the calculated ones. The results thus indicate that the Mode I mechanism needs to be modified in order to account for the large discrepancy that exists between calculated and observed critical current densities.

It is difficult to envisage that anomalously high viscosities for sodium (e.g., due to impurities or to some geometrical restrictions in the capillary channel) could account for the discrepancy; rather, the results indicate that the effective critical stress intensity factor, K_{IC}^{eff} is not the same as the one that is appropriate for mechanical testing, K_{IC}. The results require that K_{IC}^{eff} is about equal to $0.1\ K_{IC}$. Processes are, therefore, thought to occur at the crack tip that bring the critical stress intensity factor significantly below the mechanical K_{IC}. One such process is the local injection of electrons from the sharp, sodium filled crack tip. The field at the crack tip, E_o, is about $E_\infty \ell/r$. From the observation of De Jonghe et al. [2], it is clear that r can be as low as 10Å. E_o can thus easily reach local values of 10^5 V/cm (for E_∞ = 10V/cm and L = 10 μm), which may indeed lead to profuse local field injection of electrons. This process would introduce significant electronic conductivity in the ceramic in the immediate vicinity of the crack tip, leading to sodium deposition under pressure just ahead of the crack tip [1]. This effect could lead to crack growth at some critical field that is reached when the macroscopic current density is well below the one at which the mechanical stress intensity factor K_I would exceed the critical stress intensity factor, K_{IC}.

5. ACKNOWLEDGEMENTS

This work was supported by the Electric Power Research Institute.

Additional support was received from the Assistant Secretary for Conservation and Solar Energy, Office of Advanced Conservation Technology, Electrochemical Systems Research Division of the U.S. Department of Energy under Contract No. W-7405-ENG-48.

References

1. L.C. De Jonghe, Leslie Feldman, A. Buechele, J. Mat. Sci., in press.

2. L.C. De Jonghe, L. Feldman, P. Millett, Mat. Res. Bull., 14 (1979), 589-595.

3. R.D. Armstrong, T. Dickinson, J. Turner, Electrochimica Acta, 19 (1974), 187.

4. D.K. Shetty, A.V. Virkar, R.S. Gordon in Fracture Mechanics of Ceramics, V. 4, Proceedings of an International Symposium on Fracture Mechanics of Ceramics, ed. R.C. Bradt, et al, 1978, pp. 651-665.

5. P. Moon, and D. Spencer, "Field Theory for Engineers", D. Van Nostrand, Princeton, 1961.

6. R. H. Richman, and G.J. Tennenhouse, J. Am. Cer. Soc., 58 (1975), 63-67.

7. G.C. Sih, Handbook of Stress-Intensity Factors, Lehigh University Press, 1973.

8. S. Timoshenko, "Strength of Materials", Part I, 3rd Edition, D. Van Nostrand Co., Inc., Princeton, 1958.

9. A.V. Virkar, L. Viswanathan, P.R. Biswas, J. Mat. Sci., 15 (1980), 302-308.

10. J.C. Jaeger, Elasticity, Fracture and Flow, Methuen and Co., London, 1974.

TABLE I

CALCULATED VALUES OF ℓ, J_∞ AND K_I/K_{IC}

$\ell(\mu m)$	$j_\infty(A/cm^2)$	K_I/K_{IC}
10	0.1	0.025
	10	0.08
	1000	0.25
100	0.1	0.045
	10	0.14
	1000	0.45
1000	0.1	0.08
	10	0.25
	1000	0.8

$j_\infty = K_I^4 E'^3 ne/(3.32\tau\ell)$

$K_{IC} \simeq 1.6$ MPa $m^{1/2}$, Shetty et al. [4]

TABLE II

MICROCRACK SIZE, L_C,V, CRITICAL CURRENT DENSITY, j_{crit}, AND CRITICAL ZONE SIZER, FOR $j_\infty = 1 A/cm^2$, $\ell = 1cm$, AND $r/\ell = 10^{-7}$

L_c (μm)	J_{crit} (A/cm^2)	R(cm)
10	2.5×10^5	8×10^{-12}
100	2.5×10^4	8×10^{-10}
1000	2.5×10^3	8×10^{-8}

Appendix A

The crack opening displacement is calculated using a method based on the Theorem of Castigliano [8]. Fictitious forces P are applied to opposite sides of the crack and later set to zero at the location where the crack opening displacement is to be calculated. The forces are applied in this case at the opening of the elliptic-cylindrical crack. The displacement r is found to be

$$r = \frac{\partial \bar{U}_e}{\partial P} \tag{A1}$$

where $\bar{U}_e$ is the elastic strain energy and P is allowed to tend toward zero. $\bar{U}_e$ is expressed in terms of the previously calculated K_I and the stress intensity factor due to the fictitious forces. The total stress intensity factor is

$$K_I' = K_I + \frac{P}{(\pi \ell)^{1/2}} \tag{A2}$$

$\bar{U}_e$ is found from the strain energy release rate, G,

$$\bar{U}_e = \int_0^{\ell} G d\ell \tag{A3}$$

Using the relation between K_I and G (plane strain)

$$G = \frac{K_I'^2}{E'} \tag{A4}$$

we have

$$\bar{U}_e = \frac{1}{E'} \int_0^{\ell} \left(K_I + \frac{P}{(\pi \ell)^{1/2}} \right)^2 d\ell \tag{A5}$$

Using A1 and A5, differentiating and setting P = 0 before integrating,

$$r = \frac{2}{E'}\int_0^{\ell} \left(K_I + \frac{P}{(\pi\ell)^{1/2}} \right) (\pi\ell)^{-1/2} d\ell$$

$$= \frac{2}{E'}\int_0^{\ell} \frac{K_I}{(\pi\ell)^{1/2}}\, d\ell \qquad \text{(A6)}$$

To find $r(\ell)$ from A6, we note that r is on both the left side and the right side of the equation inside the integral, since

$$K_I = \frac{11.35}{\pi}\, \tau\, \left(\frac{\ell}{r}\right)^3 \ell^{-1/2}\, \frac{j_\infty}{ne} \qquad (14)$$

We then differentiate both sides of A6 with respect to crack length and get a result of the form

$$\frac{dr}{d\ell} = k\ell^2 r^{-3} \qquad \text{(A7)}$$

where k is a constant equal to $\frac{2}{E'} \frac{11.35\tau}{\pi^{3/2}} \frac{j_\infty}{ne}$.

The solution to A7 is

$$r = \left(\frac{4k}{3}\right)^{1/4} \ell^{3/4} \qquad \text{(A8)}$$

LIST OF FIGURE CAPTIONS

Fig. 1. Current focusing geometry for elliptic-cylindrical crack.

Fig. 2. Coordinate system for elliptic-cylindrical crack.

Fig. 3. Comparison of calculated pressure distributions along crack.

Fig. 4. Geometry for elliptic-cylindrical blocking platelet.

Fig. 5. Comparison of current density and transition stress around elliptical hole in sheet.

Fig. 6. Metal-filled microcrack in enhanced current density zone.

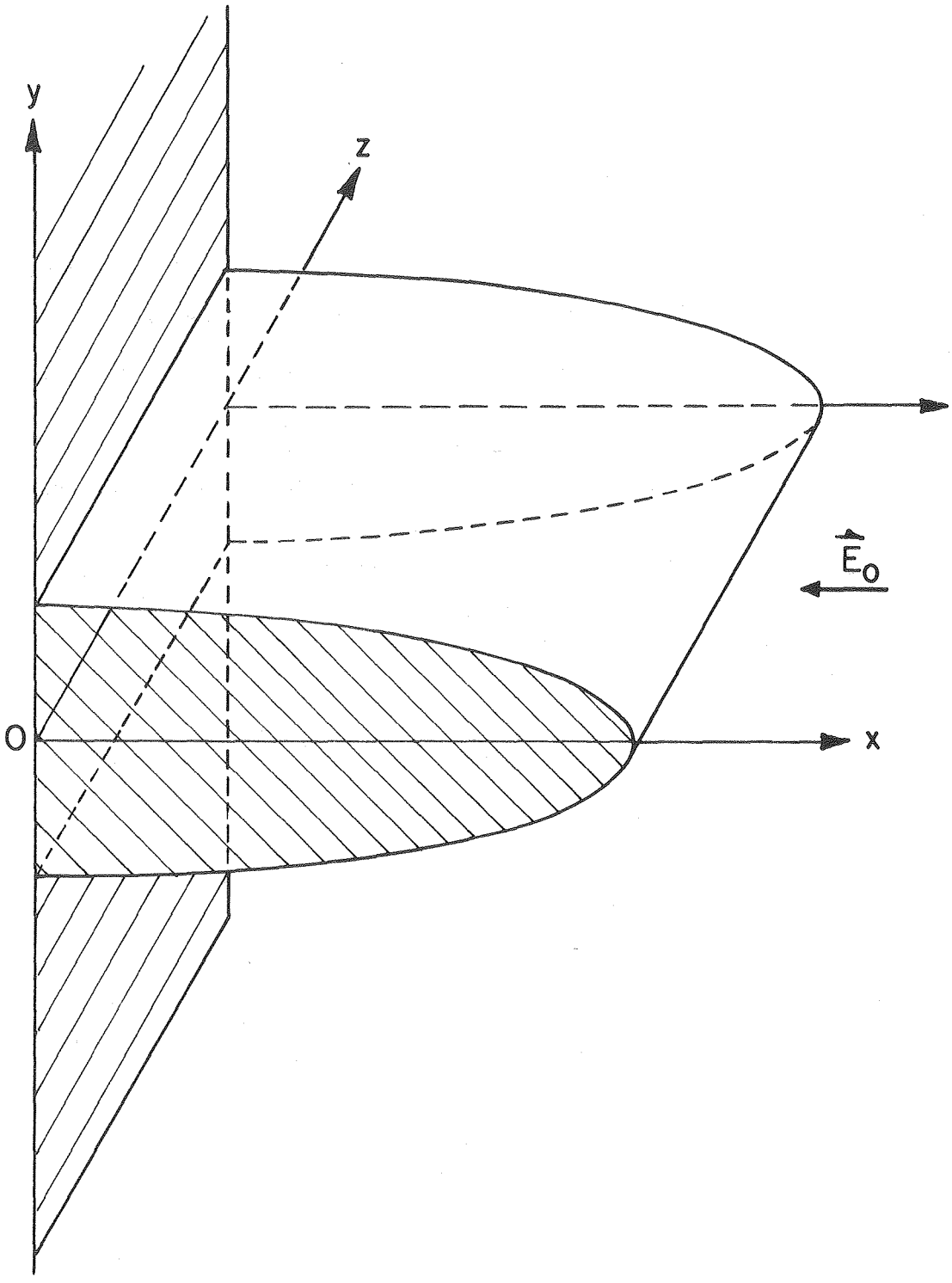

Figure 1

XBL8011-6268

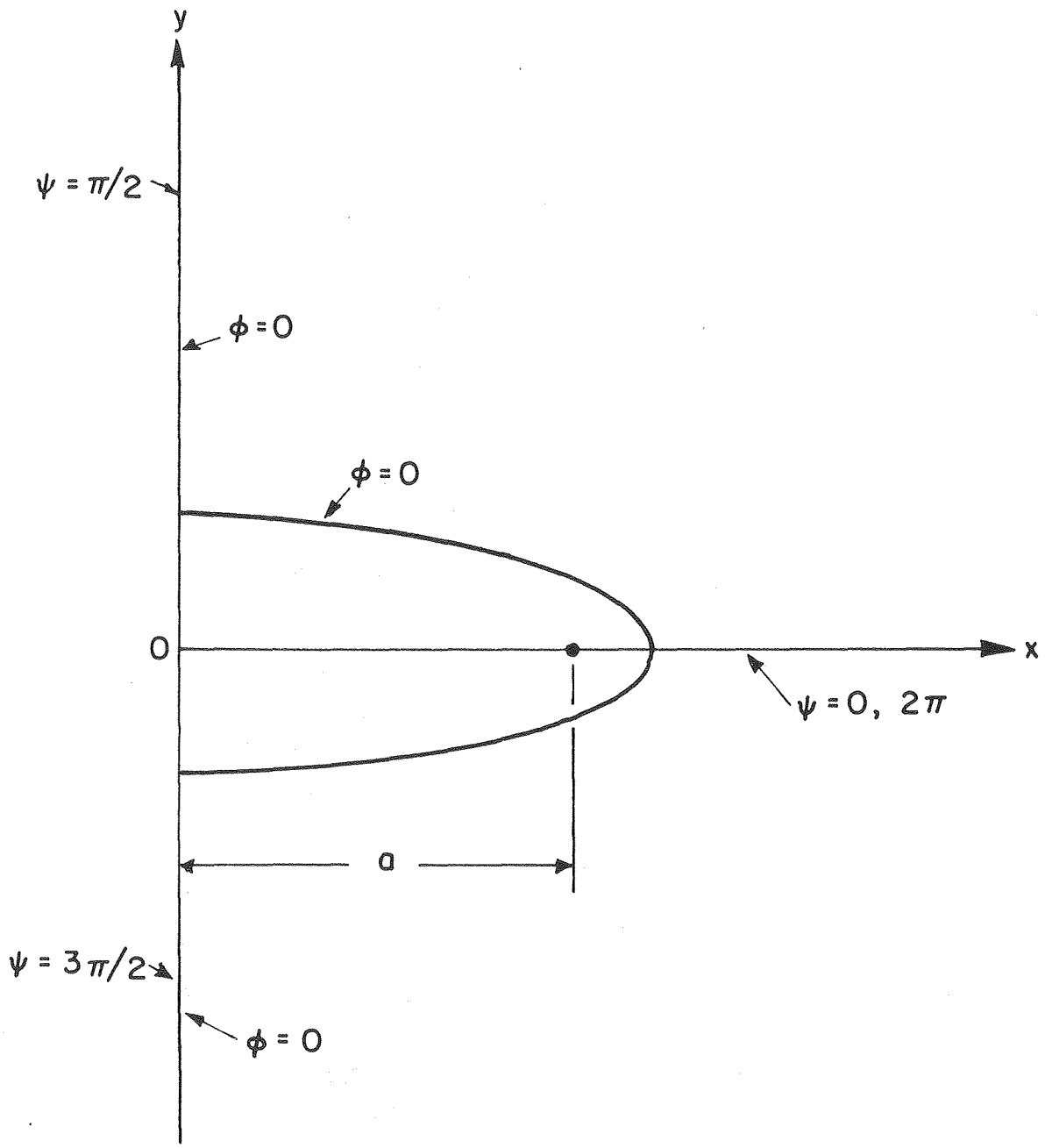

Figure 2

XBL 8011-6267

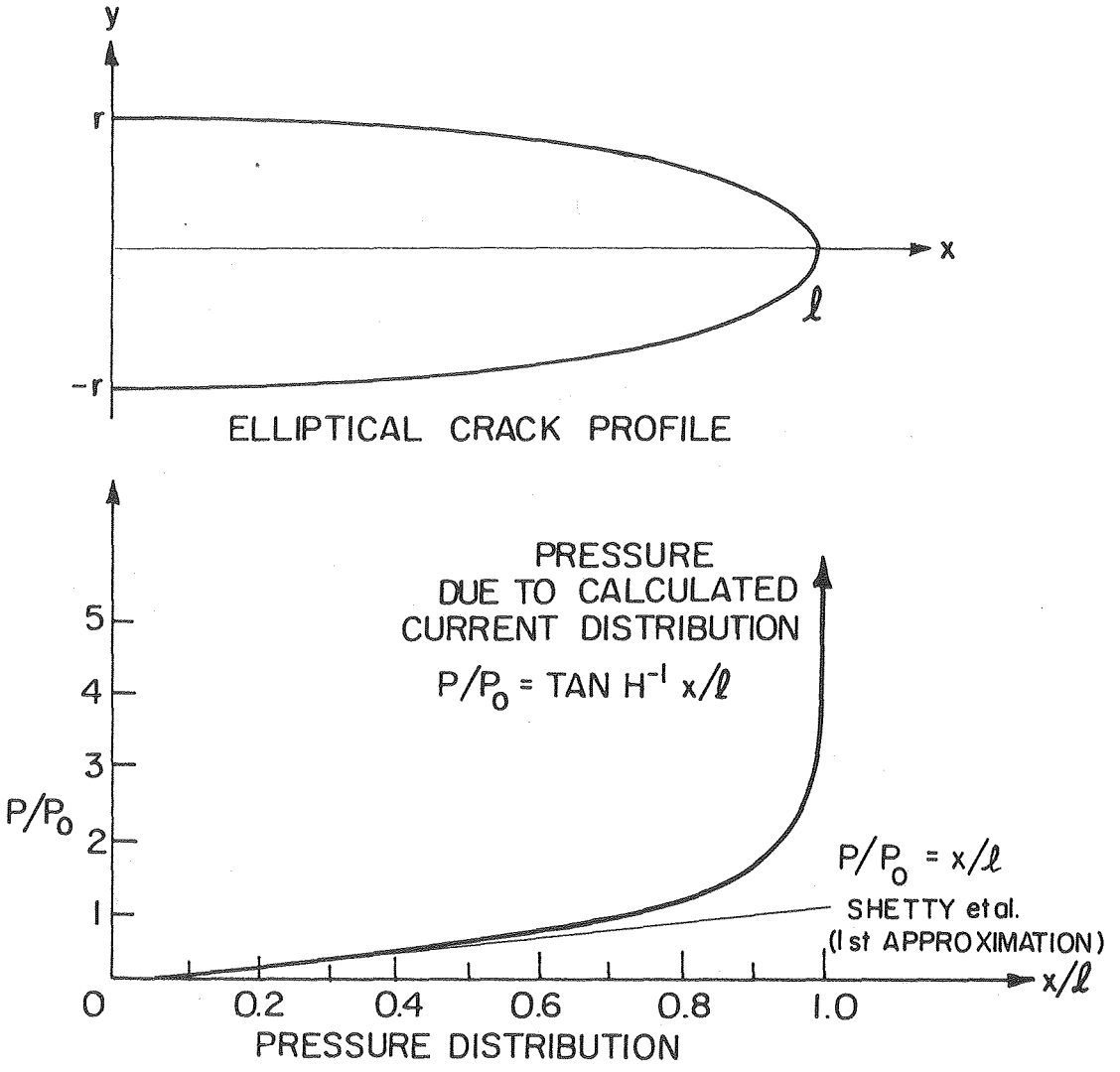

XBL8011-6266

Figure 3

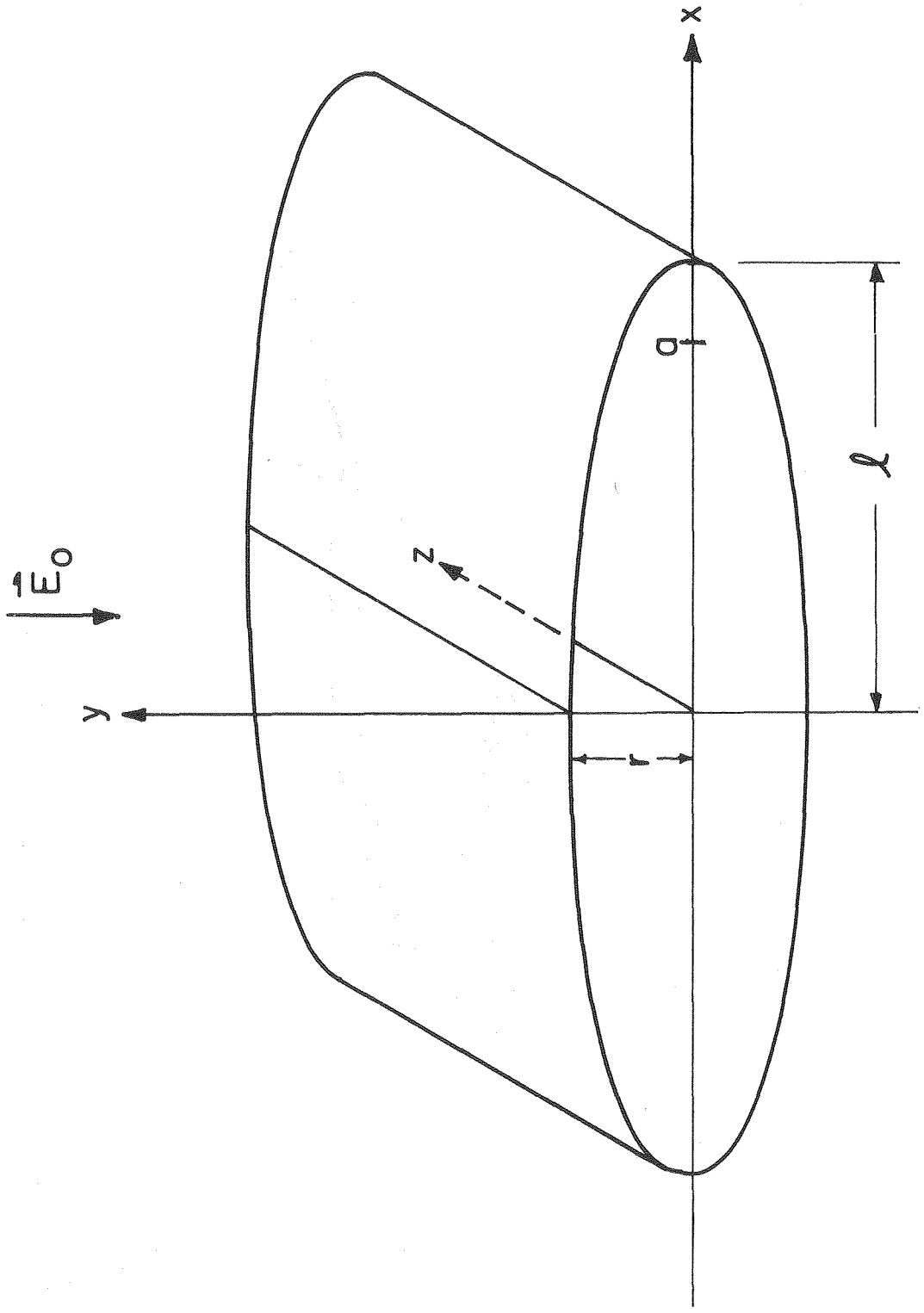

XBL 8011-6265

Figure 4

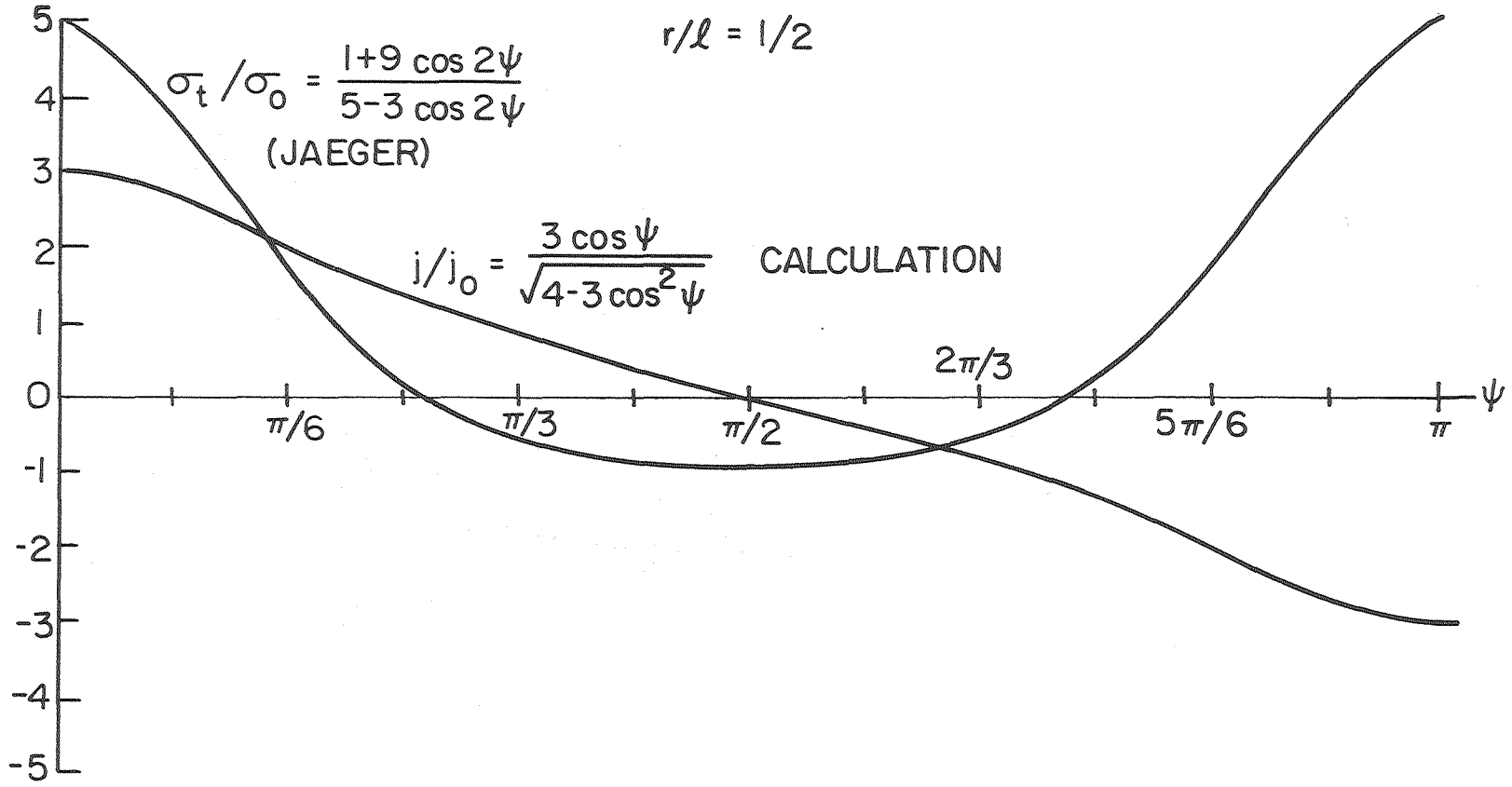

Figure 5

XBL8011-6254

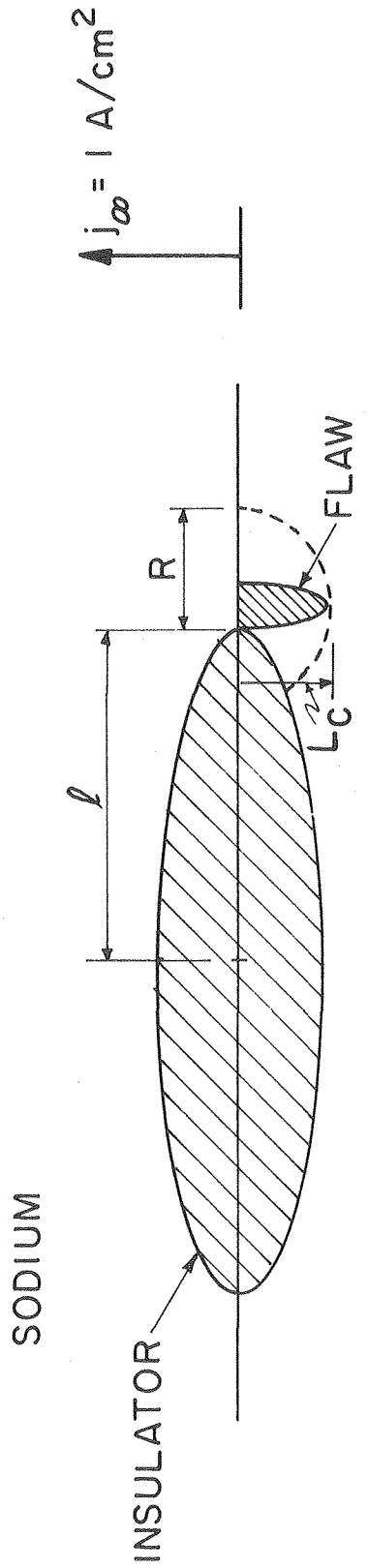

XBL 812-5202

Figure 6